Daniele Castelli · Daniela Rubatto

# Stability of Al- and F-rich titanite in metacarbonate: petrologic and isotopic constraints from a polymetamorphic eclogitic marble of the internal Sesia Zone (Western Alps)

**Abstract** Al- and F-rich titanite $(3.86 < Al_2O_3 < 9.33$ wt%, $0.93 < F < 2.53$ wt%) from a polymetamorphic marble of the Sesia Zone (Western Alps) has been investigated in order to determine the behaviour of titanite during high-pressure metamorphism. Meso-structural to micro-structural relationships, mineral assemblages and petrological data indicate a pre-Alpine (low-pressure, high-temperature) to early-Alpine (high-pressure, medium-temperature) pressure–temperature–time evolution. Backscattered electron images, X-ray qualitative elemental maps and electron microprobe analysis show that most Al- and F-rich titanite that occurs as isolated crystals is rather homogeneous in composition. In contrast, titanite associated with, or rimmed by, typical early-Alpine, high-pressure minerals is characterized by variable $Al_1(F, OH)_1Ti_{-1}O_{-1}$ substitution within single crystals, particularly at grain boundaries with omphacite and/or phengite. In-situ ion microprobe U–Pb analysis of titanite domains that have various Al and F contents yielded apparent $^{206}Pb/^{238}U$ ages scattering between 283 and 153 Ma. Chemical and petrological data are indispensable to interpret this complex age distribution, and the good correlation between $^{206}Pb/^{238}U$ ratios and Al content indicates that the Al- and F-rich titanite was formed during pre-Alpine metamorphism $(\geq 281 \pm 11$ Ma). Progressively younger ages are obtained in domains with decreasing Al and F content, suggesting that partial chemical re-equilibration was responsible for the incomplete isotopic resetting during Alpine metamorphism. Petrological and U–Pb data show that Al- and F-rich titanite should be used with caution to infer high-pressure conditions in polymetamorphic carbonate systems.

## Introduction

Titanite is a common accessory mineral in magmatic and metamorphic rocks, and has been also reported from eclogites and associated high pressure (HP) to ultrahigh pressure (UHP) calc-silicates and marbles (see Enami et al. 1993 for a review). Both natural occurrence (e.g., Smith 1977, Smith and Lappin 1982; Franz and Spear 1985; Sobolev and Shatsky 1990; Hirajima et al. 1992; Carswell et al. 1996; Ye and Ye 1996) and experimental data (Smith 1980, 1981; Troitzsch and Ellis 1999) show that many HP to UHP titanites are enriched in $Al_2O_3$ and fluorine. The highest $Al_2O_3$ content recorded in eclogite-facies marbles ($\sim$14.1 wt%, Franz and Spear 1985) is close to the experimentally observed limit of $X_{Al} = Al/(Ti + Al + Fe^{3+}) = 0.50 \pm 0.03$ (Smith 1981), although Troitzsch and Ellis (1999) recently synthesized $CaAlFSiO_4$, the Al–F analogue of titanite. Al- and F-rich titanite has also been reported from low-pressure (LP) metamorphic rocks, showing that the $(Al, Fe^{3+})FTi_{-1}O_{-1}$ substitution also controls the Al content of titanite under high-temperature conditions (Enami et al. 1993; Markl and Piazolo 1999). Compilations by Oberti et al. (1991) and Enami et al. (1993) also show that $Al_2O_3$-free metamorphic titanite does not seem to exist. These data emphasize that Al and F contents of titanite alone do not provide simple and straightforward estimates of P–T conditions, but are controlled by the activity of F and bulk-rock composition (Franz and Spear 1985; Enami et al. 1993; Carswell et al. 1996; Markl and Piazolo 1999).

D. Castelli (✉)
Dipartimento di Scienze Mineralogiche e Petrologiche, Università di Torino,
Via Valperga Caluso 35, Torino, Italy
E-mail: castelli@dsmp.unito.it

D. Rubatto
Research School of Earth Sciences,
The Australian National University,
Canberra 0200 ACT, Australia

Editorial responsibility: J. Hoefs

Titanite in both magmatic and metamorphic rocks can contain small amounts of U and is, therefore, an important mineral for U–Pb geochronology (Frost et al. 2000). Experimental (Cherniak 1993), theoretical (Dahl 1997) and geochronological studies (e.g. Schärer et al. 1994; Pidgeon et al. 1996; Verts et al. 1996; Essex and Gromet 2000; Rubatto and Hermann 2001) have demonstrated that titanite is able to retain its U–Pb composition at temperatures as high as 750 °C. This implies that titanite formed at different stages during a metamorphic cycle can potentially retain its original U–Pb age. Dating of such titanite is thus an important tool for the construction of P–T–time paths. Multi-stage growth of titanite has been documented in a contact aureol (Verts et al. 1996) and amphibolite-facies gneisses (Essex and Gromet 2000) using colour, morphology and chemical composition as discriminat-ing factors. Sensitive high-resolution ion microprobe analysis allowed Rubatto and Hermann (2001) to date directly, in thin section, titanite domains of different composition and inclusions, which formed during Al-pine metamorphism at UHP peak conditions (750 °C and 35 kbar) and two retrograde stages. They could even identify relict titanite cores still preserving a pre-Alpine age.

Because it can be precisely dated by U–Pb, titanite bears a great potential for constraining pressure–temperature–time paths, particularly in HP rocks. However, in order to fully exploit this potential, our knowledge of titanite stability and isotopic as well as chemical composition under variable P–T conditions needs to be improved. We investigated the chemistry and metamorphic history of selected titanites in a polymetamorphic marble from the Sesia Zone of lower Aosta Valley (Western Alps) with a new approach that combines petrologic, back-scattered electron, and elec-tron microprobe analysis with X-ray qualitative ele-mental mapping and sensitive high-resolution ion microprobe (SHRIMP) isotopic measurements. Our multidisciplinary approach and, particularly, the wide application of in-situ microanalysis, allowed us to constrain the chemical and isotopic behaviour of tita-nite that underwent polymetamorphism at different pressures and temperatures. The new petrologic, chemical and isotopic data indicate that Al- and F-rich titanite should be used with caution to infer HP con-ditions and have important implications for U–Pb geochronology.

## Geological setting

The internal Sesia Zone is a slice of pre-Alpine continental crust composed of high-grade paragneiss, amphibolite and minor mar-ble, which was intruded by late-Variscan granitoids (Compagnoni 1977; Compagnoni et al. 1977; Oberhänsli et al. 1985; Droop et al. 1990). The high-temperature (HT) pre-Alpine metamorphism is constrained at T = 730–830 °C, P = 7–9 kbar (Lardeaux and Spalla 1991). This metamorphism is Variscan in age according to a $273 \pm 16$-Ma Ar–Ar age of mica from pre-Alpine micaschists

(Reddy et al. 1996) and a post-metamorphic intrusion dated at $294 \pm 3$ Ma (Rubatto 1998).

The early-Alpine HP metamorphism is constrained at T = 500–600 °C and P = 13–20 kbar (Compagnoni 1977; Koons 1982; Lar-deaux et al. 1982; Droop et al. 1990). P–T peak estimates and the P–T–t path related to post-peak re-equilibration under blueschist to greenschist facies conditions have been discussed by Lardeaux et al. (1982), Pognante (1989, 1991) and Droop et al. (1990). The early-Alpine HP stage has been recently dated at $69.2 \pm 2.7$ Ma (Lu–Hf phengite–garnet ages: Duchêne et al. 1997), ~65 Ma (U–Pb SHRIMP zircon ages: Rubatto et al. 1999), and 60–70 Ma (Rb–Sr white mica and U–Pb titanite ages: Inger et al. 1996). Inger et al. (1996) obtained different U–Pb titanite ages from polymetamorphic rocks, but a concordant age of $66 \pm 1$ Ma from monometamorphic assemblages. They interpreted this age as dating the Alpine HP metamorphism and concluded that Pb inheritance in titanite was preserved at temperatures of 600 °C. In contrast, Schärer et al. (1999) obtained unexpectedly old U–Pb titanite ages from three Sesia marbles ($278 \pm 2$, 241–226 and 201–180 Ma, respectively), which were considered to contain an HP Alpine assemblage. The same authors measured much younger Rb–Sr ages between 55 and 48 Ma in phengite from the same samples, suggesting a younger age for the metamorphism.

Phengite $\pm$ omphacite, garnet, and titanite-bearing marbles of the internal Sesia Zone occur as centimetre- to several metre-thick lenses and/or discontinuous layers within the paragneiss. The marbles record the same Alpine polyphase evolution as the country rocks (Compagnoni 1977; Castelli 1991). The HP stage in the marbles is constrained at T = $575 \pm 45$ °C, P≥15 kbar (which is in agreement with P–T estimates in felsic rocks and eclogite, e.g. Droop et al. 1990), and an early retrograde stage occurred at T ≤ 500 °C, P(H$_2$O)≥9 kbar (Castelli 1991). Modelling of phase equilibria suggests that mineral assemblages coexisted with aque-ous fluids ($X(CO_2) \leq 0.03$) during their entire Alpine evolution (Castelli 1991). Castelli (1991) argued that the Al- and F-rich (up to 8.5 wt% Al$_2$O$_3$ and 2.9 wt% F), coarse-grained porphyroblastic to porphyroclastic titanite formed at the HP stage, whereas the fine-grained, idiomorphic titanite (with low-Al contents: Al$_2$O$_3$ < 4.0 wt%) formed during late LP re-equilibration.

Despite extensive Alpine tectono-metamorphic reworking, and because of the different rheology between carbonate and silicate minerals, relics of pre-Alpine fabric and mineral assemblages lo-cally occur. Based on these relics, petrologic data from marbles of the Ivrea Zone (Papageorgakis 1961) and pre-Alpine P–T estimates in the country rocks, HT pre-Alpine assemblages in marbles of the internal Sesia Zone probably consisted of calcite–dolomite $\pm$ quartz, plagioclase, Ca-pyroxene, Ca-amphibole, biotite, phlogo-pite and titanite (Castelli 1987, 1991).

## Analytical techniques

Mineral spot analyses were performed on selected polished thin sections with a LINK-EDS-equipped Cambridge scanning electron microscope (SEM) at the Department of Mineralogic and Petro-logic Sciences, University of Torino. Natural silicates and oxides were used as standards, and as monitors to check the accuracy of measurements. The accelerating voltage was 15 kV and the inte-gration time was 50 s. At the location of ion microprobe mea-surements in titanite, several spot analyses were performed within the ion microprobe pits in order to detect any small-scale zoning. The F content in titanite was measured only for selected spot an-alyses and, because of both low X-ray count rates for F and their rapid fall-off with time, the F values have a relatively large un-certainty. However, the F content detected in titanite crystal #1821.1 (0.104 < F < 0.189, av. 0.146 p.f.u.) closely matches that previously measured in the same crystal by using a WDS microp-robe (0.094 < F < 0.183, av. 0.134; detection limit is 0.08 wt% and relative error is 10.0%: Castelli, unpublished data; see Castelli 1991 for details on analytical techniques). The titanite formulae were calculated according to the procedure described in Oberti et al.

(1991), which assumes full occupancy of the Ca, Si and Ti sites, and that all Fe is present as $Fe^{3+}$. Following the approach of Oberti et al. (1991) and Markl and Piazolo (1999), only the Si, Ti, Al, Fe, Ca and F values have been considered in the formula calculation, since minor elements such as Mn, Mg and Na are always <0.1 wt% on average, and some Cr was only detected in one sample (see below).

Qualitative elemental (Si, Al, Ti, Fe, Mg Ca and F) X-ray maps of titanite crystals were recorded by the same equipment, using the approach of Borghi et al. (1998). The resolution of each mapped area was 512×512 pixels, with a dwell time of 40 ms for each pixel. A back-scattered electron (BSE) investigation was carried out at the Electron Microscope Unit at the Australian National University, with a Cambridge S360 SEM using a voltage of 20 kV, a variable current between 3 and 6 nA and a working distance of ~20 mm.

Titanite was analysed for U, Th and Pb using the sensitive high-resolution ion microprobe (SHRIMP II) at the Australian National University. Data acquisition and reduction were similar to the methods used for zircon (Compston et al. 1992). The $^{206}Pb/^{238}U$ ratios were calibrated against a Kham titanite standard (518 Ma, Kinny et al. 1994). Analyses were performed directly in thin sections in order to preserve textural information. A correction for common Pb was done according to the measured $^{204}Pb$. Similar values were obtained using a common Pb correction based on the $^{208}Pb/^{206}Pb$ ratio (Compston et al. 1992). Because the data obtained do not form a cluster, the common Pb composition could not be obtained from the $^{207}Pb/$ $^{206}Pb–^{238}U/^{206}Pb$ isochron (e.g. Rubatto and Hermann 2001). Therefore, for each data point, common Pb was assumed to have the composition predicted by the Pb growth curve of Stacey and Kramer (1975) at 283 Ma, the oldest age measured and the minimum age for the titanite crystallization. This method, although not rigorous, is preferred to the measurement of common Pb from phases such as calcite, which cannot be proven to be in isotopic equilibrium with the titanite, in particular with composite titanite as found in the Sesia marbles. In fact, these marbles experienced HP Alpine metamorphism in the aragonite stability field, and petrographic evidence suggests that the retrograde calcite recrystallized during late Alpine overprint, whereas the tita-

nite is largely a relic of the Variscan paragenesis. Moreover, most of the SHRIMP analyses contain a small amount of common Pb and, therefore, different common Pb compositions would only account for a small variation in age, without affecting our conclusions. The good correlation between $X_{Al}$ and $^{206}Pb/^{238}U$ is a further indication that the common Pb correction adopted is appropriate.

# Petrography

The hand-specimen was collected in the lower Aosta Valley, at the bottom of a rock-wall that occurs along the right side of the Dora Baltea River, about 500 m

**Fig. 1 a** Hand-specimen of the polymetamorphic marble consisting of yellowish carbonate-rich layers (*dark in photograph*) that alternate with whitish qtz–phengite-rich layers. A porphyroclast of salitic augite (Aug) at *bottom-right* is partly replaced in the rim by the high P Na–Cpx + Grt assemblage. *Darker spots* (*black arrows*) in the carbonate layers are the omphacite ± phengite ± titanite-bearing silicate aggregates. *Boxes* outline the area of polished thin sections, including #SL1821 and #SL1823/PA samples that have been selected for this study. **b** Euhedral (associated with omphacite) to subhedral titanite crystals in a carbonate-rich layer that wraps around a relict salitic augite (at top). **c** Relict augite within a quartz + calcite ± titanite matrix; note inclusions of subhedral titanite, and the Na-augite developing at rim (*dashed line*) of salitic augite. **d** Apparent textural equilibrium between omphacite, phengite, and anhedral, fractured titanite in a porphyroclastic domain within a calcite layer. Calcite in **b** and **d** is darker because of staining technique. The attitude of high P foliation in photomicrographs **b**, **c**, and **d** is horizontal as in **a**. Mineral abbreviations according to Kretz (1983), except for *Ph*phengite and *Omph* omphacite
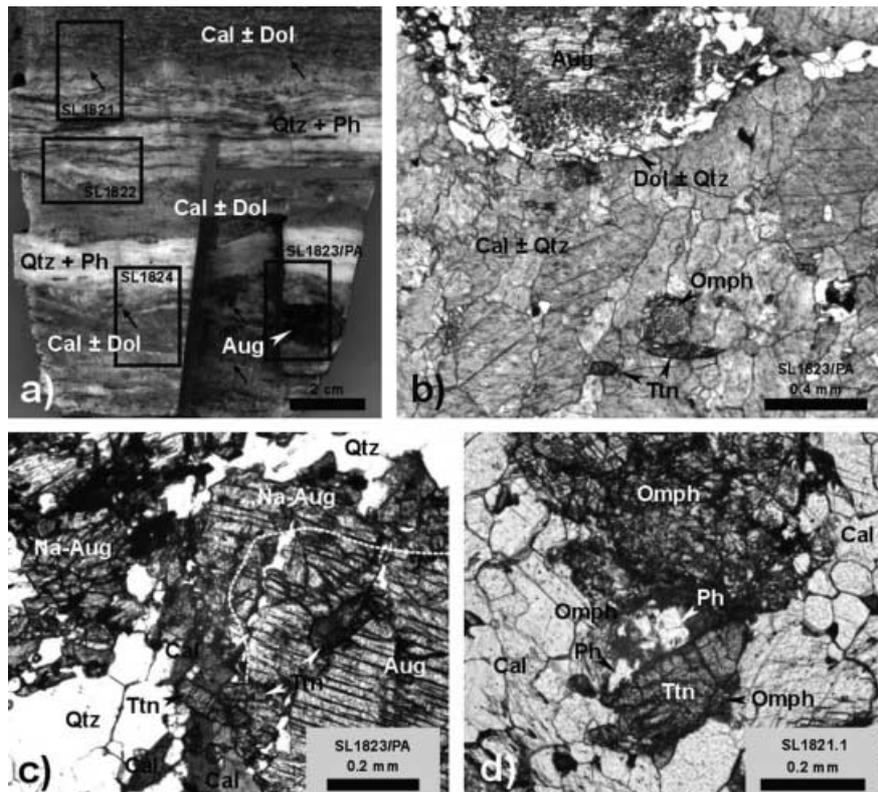
**Fig. 2** BSE images and Al, Ti qualitative X-ray maps of four (**a–d**) selected titanite-bearing domains. Details of titanite textures are given in Table 1. Areas with high BSE emission correlates with high Ti content (*light grey* in the Ti X-ray maps). *Circles* within BSE images are SHRIMP analysis pits for which single ages ($\pm 1\sigma$) are given. The Al and Ti X-ray maps also show compositions of minerals associated with titanite, location of titanite spot analyses (*full dots*), the $X_{Al} = Al/(Al + Fe^{3+} + Ti)$, and $X_{Ti} = Ti/(Al + Fe^{3+} + Ti)$ values, and the F p.f.u. contents (*italic within brackets*). Averaged values are given at SHRIMP pits; abbreviations as in Fig. 1. See text for discussion
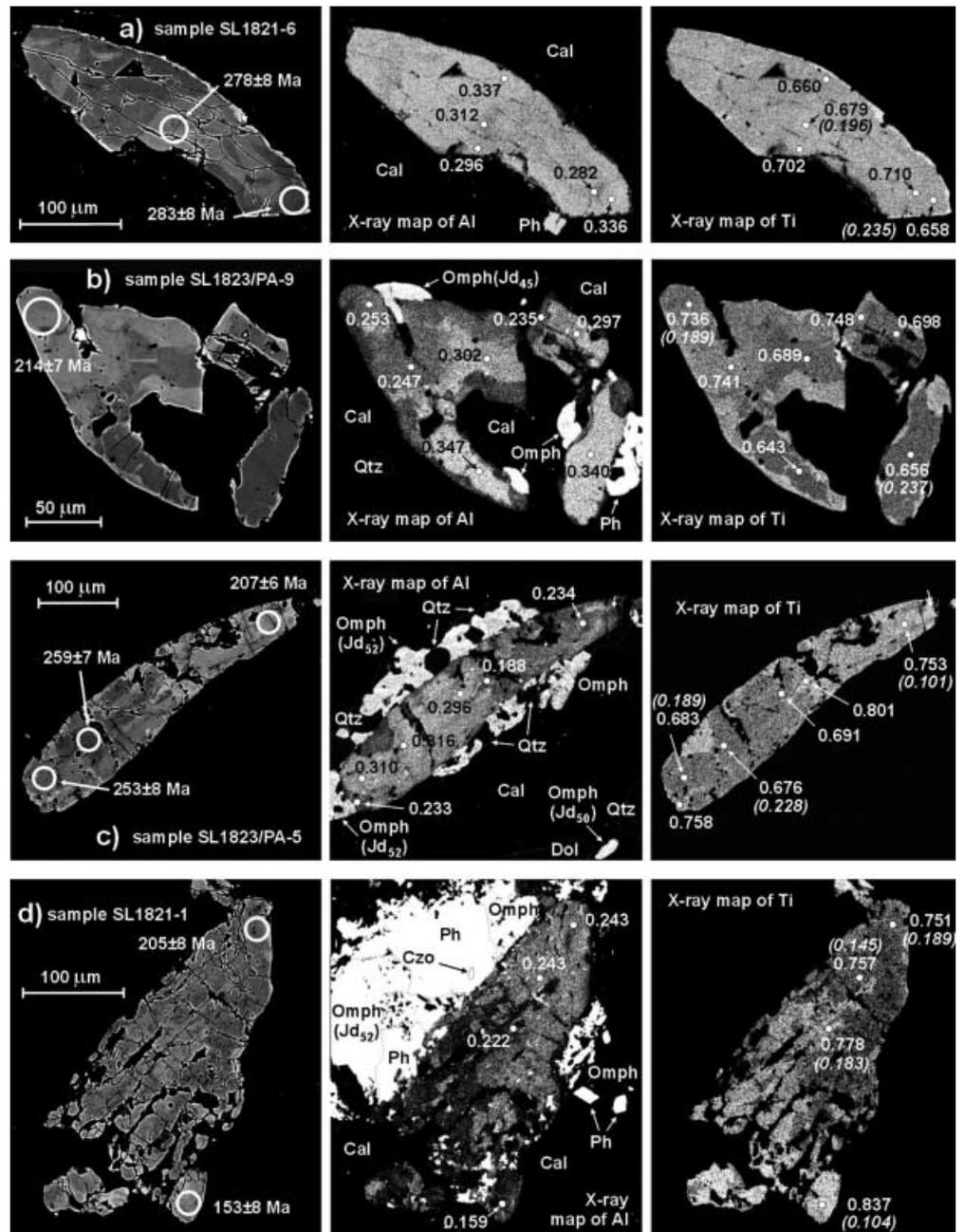


south of Pont St. Martin. The lower part of rock-wall consists of poly-deformed omphacite–garnet–phengite ± glaucophane-bearing paragneiss, which hosts metre-thick eclogite boudins and marble layers and/or lenses (Compagnoni 1977; Castelli 1987, 1991).

The specimen consists of yellowish carbonate-rich layers that alternate with whitish quartz–phengite-rich layers (Fig. 1a). The contact between layers is sharp and runs parallel to the main regional foliation, which correlates with the HP metamorphic event (Passchier et al. 1981; Williams and Compagnoni 1983; Castelli 1991). In the quartz–phengite layers, quartz occurs as continuous ribbons of recrystallized subgrains that alternate with fine-grained phengite sub-layers. Locally, the foliation

wraps around fine- to medium-grained, porphyroblastic to porphyroclastic omphacite, zoisite and very minor titanite.

The medium- to fine-grained carbonate layers consist of granoblastic calcite, with minor quartz and rare dolomite. These layers retain scattered silicate-rich domains whose mineralogy is comprised of clinopyroxene, garnet, epidote minerals, phengite and titanite (Fig. 1b, c). The multistage evolution of these silicate domains is described in Castelli (1987, 1988, 1991) and summarized here. Large porphyroclasts of colourless salitic augite ($Wo_{49}En_{26}Fs_{22}Acm_3$) are relics of the pre-Alpine metamorphic evolution (Fig. 1b). They are partly replaced at the rim by HP minerals such as pale-green Na-augite

**Table 1** Mineral assemblages and textural description of selected titanite-bearing domains. The minerals listed (in order of decreasing abundance) are not all in equilibrium at the same P–T conditions. *Omph* Omphacite; *Ph* phengite; other abbreviations after Kretz (1983). Zoning of titanite refers to $Al_2O_3$ content

| Domain no. | Minerals present | Titanite textures | Fig. 2 |
|---|---|---|---|
| SL1821-1 | Cal, Omph, Ph ± Czo | Anhedral, fractured crystal in an omphacite + phengite-bearing porphyroclastic domain within a calcite layer; irregularly zoned. Apparent equilibrium boundary to phengite, omphacite at rim; small calcite inclusions | b |
| SL1821-6 | Cal, Ph | Euhedral, weakly zoned crystal in a calcite matrix, parallel to the foliation. Very minor phengite at rim | c |
| SL1821-8 | Cal | Subhedral, weakly zoned crystal in a calcite matrix, parallel to the foliation | |
| SL1823/PA-1 | Qtz, Cal, Czo | Homogeneous, subhedral, fractured crystals in a quartz domain as pressure shadow around a salite porphyroclast; crystals parallel or at small angle to the foliation. Calcite along cracks and minor epidote along cracks and at rims | |
| SL1823/PA-5 | Cal, Omph, Qtz ± Dol | Subhedral, deformed crystal in a calcite (plus very-minor dolomite) matrix; patchy zoned and parallel to the foliation. Fine-grained, discontinuous corona of omphacite and quartz | d |
| SL1823/PA-8 | Cal | Homogeneous, subhedral, fractured crystal in a calcite matrix, at small angle to the foliation | |
| SL1823/PA-9 | Cal, Omph, Ph, Qtz | Anhedral, corroded crystals in a calcite matrix; irregularly zoned. Very fine-grained phengite and/or omphacite at rims or along small cracks | a |

$(Wo_{44}En_{25}Fs_{14}Acm_{8-15}Jd_{2-9})$ and minor yellowish garnet $(Alm_{61}Gro_{22}Sps_8Prp_5Adr_4)$, and locally retain Cl-, F-bearing amphibole and biotite and subhedral titanite (Fig. 1c). Aggregates of granoblastic omphacite (up to $Jd_{52}$) ± phengite $(3.34 < Si < 3.38$ p.f.u.), quartz and rare garnet are also part of the HP stage. Isolated porphyroclastic garnet is also found. Geothermometric estimates from coexisting clinopyroxene and garnet at the rim of pre-Alpine salite yield $T = 573 \pm 23$ °C and $T = 553 \pm 23$ °C at $P = 18$ kbar (calibrations of Ellis and Green 1979 and Powell 1985, respectively), in agreement with previous T estimates by Castelli (1991).

As in all Sesia marbles (Castelli 1991), no rutile has been observed and titanite is the accessory Ti-phase that is stable during all metamorphic stages. Figures 1 and 2 show some representative titanite textures, and Table 1 summarizes the minerals and textures in the titanite-bearing domains that were selected for the chemical and isotopic investigations. Titanite occurs as subhedral (Figs. 1b and 2a) to anhedral (mostly fractured and/or deformed) crystals (Figs. 1d, 2b, c). Most of them are optically and chemically inhomogeneous with complex zoning (Fig. 2). Crystals are both isolated within the carbonate matrix (Figs. 1b and 2a) and associated with omphacite ± phengite and quartz (Figs. 1d, 2b–d). The isolated titanite crystals in the carbonate matrix are mostly pre-kinematic and partly rotated according to the main foliation (Fig. 1b), as well as some deformed and fractured titanite in small, quartz-rich domains that occur as pressure shadows around the porphyroclastic augite. Titanite + omphacite ± phengite are either in apparent textural equilibrium (Figs. 1d and 2d), or very fine-grained omphacite ± quartz occur at the rim and along cracks of titanite (Fig. 2b, c). Both these omphacite types are rather homogeneous in composition $(0.45 < X_{Jd} < 0.52)$, and the phengite shows Si $\sim 3.36$ p.f.u. Scanty clinozoisite–epidote $(Zo_{65}Ep_{35})$ is associated with the omphacite + phengite + titanite domains (Fig. 2d), or occurs as fine-grained, weakly zoned crystals $(Zo_{58-63}Ep_{42-37})$ at the rim and along cracks of isolated titanite. Neoblastic, fine-grained titanite (similar to the late, euhedral and Al-poor titanite of Castelli 1991, see also $Ttn_2$ in Fig. 3) is rare.

## Chemical and isotopic composition of titanite

Chemical and isotopic investigations have been carried on representative titanite-bearing domains (Table 1) that have been selected from samples SL1821 and SL1823/PA (see Fig. 1a for their meso-structural relationships). Representative titanite compositions are given in Table 2 (the complete titanite analyses data set is provided as ESM in Table e1), and all data are plotted in Figs. 3 and 4.

Spot analyses and X-ray elemental maps show that the Ca content in titanite crystals from both samples is homogeneous and close to ideal occupancy (averaging 0.995 and 0.992 p.f.u. in samples SL1821 and SL1823/PA, respectively). Calculated Si occupancies at the tetrahedral site are slightly lower in sample SL1821 (av. = 0.975 p.f.u.) with respect to SL1823/PA (av. = 0.993), but the Si X-ray maps barely show any significant chemical zonation in each crystal or differences between crystals. Total occupancies at the octahedral site are 0.984 and 0.992 p.f.u. on average in samples SL1821 and SL1823/Pa, respectively. Although the possibility of real vacancies cannot be ruled out (e.g. Markl and Piazolo 1999), low apparent occupancies are probably related to some Cr that has not been included in the formula calculation. In fact, titanites from sample SL1821 (which show the higher deficiency at the octahedral site) contain up to 0.42 wt% of $Cr_2O_3$ $(Cr_2O_3 = 0.15$ wt% on average), whereas Cr is always below the detection limit in titanites from sample SL1823/PA.
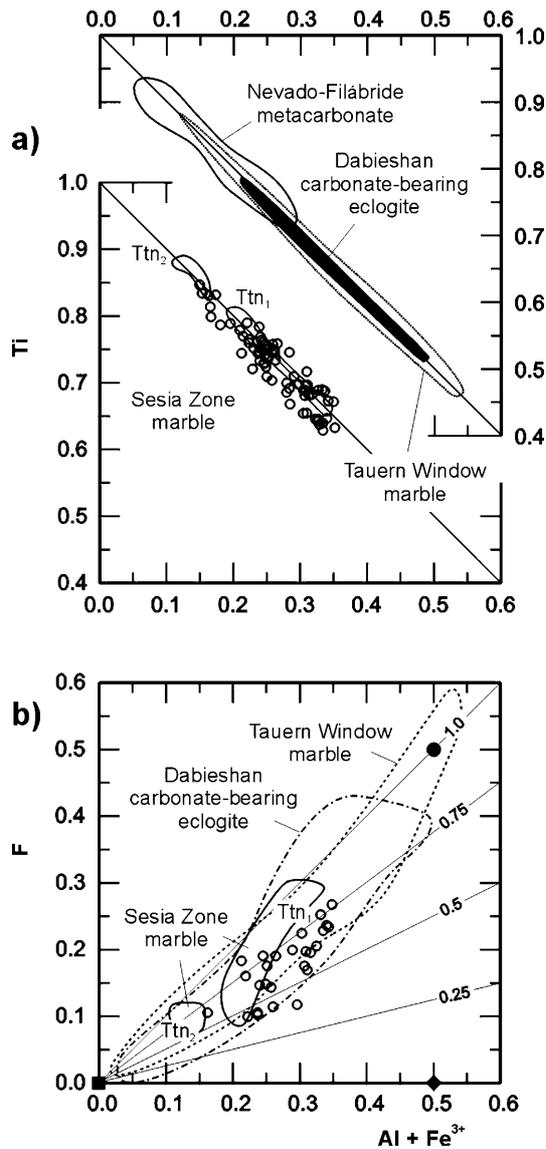
**Fig. 3** **a** Correlation between (Al + $Fe^{3+}$) and Ti (per formula unit) in titanite from studied samples (*open symbols*), compared with titanite in other marbles from the internal Sesia Zone ($Ttn_1$ and $Ttn_2$ fields, respectively: Castelli 1991), in marbles from the Eclogite Zone of Tauern Window (Franz and Spear 1985), in carbonate-bearing ultra-high pressure eclogites of Dabieshan (Carswell et al. 1996), and in carbonate rocks from the Nevado-Filábride Complex of Cordilleras Béticas (López Sánchez-Vizcaíno et al. 1997). The *straight lines* show the ideal substitution $(Al, Fe^{3+})_1(F, OH)_1Ti_{-1}O_{-1}$. **b** Correlation between F and Ti (per formula unit) in selected titanite crystals from studied samples (*open symbols*). Other data source as in **a**. The *numbered lines* indicate constant F/(F + OH) ratios. The *full square, diamond* and *dot* show location of ideal, AlOH- and AlF-titanite, respectively. See text for discussion

Based on the Al content at the octahedral site $[0.148 \leq X_{Al} = Al/(Al + Fe^{3+} + Ti) \leq 0.339$ in sample SL1821 and $0.178 \leq X_{Al} \leq 0.347$ in sample SL1823/PA], the analysed titanites fall in both the low-aluminium ($X_{Al} \leq 0.25$) and high-aluminium ($X_{Al} \geq 0.25$) titanite fields of Oberti et al. (1985, 1991). Al contents (up to 9.33 wt%) greatly exceed $Fe^{3+}$ contents, which are low

throughout the samples ($Fe^{3+} \leq 0.016$ p.f.u., av. = 0.007 in sample SL1821, and $Fe^{3+} \leq 0.017$ p.f.u., av. = 0.009 in sample SL1823/PA). The F contents (up to 2.53 wt%) average 0.183 p.f.u. ($0.104 \leq F \leq 0.251$) in sample SL1821, and 0.170 p.f.u. ($0.098 \leq F \leq 0.237$) in sample SL1823/PA. These data are evidence of a strong negative linear correlation between Ti and (Al + $Fe^{3+}$), and a positive correlation between F and (Al + $Fe^{3+}$), respectively (Fig. 3). As recognized by previous workers (e.g. Franz and Spear 1985; Oberti et al. 1991; Enami et al. 1993; Carswell et al. 1996; Markl and Piazolo 1999), these variations in Al and F (and very minor Fe) contents can be attributed to the coupled substitution

$$Ti^{4+} + O^{2-} = (Al, Fe^{3+}) + (F, OH)^+ \qquad (1)$$

that occurs at the octahedral site and at the O1 position. The extent of coupled substitution (1) in the two samples completely overlaps the $Ttn_1$ compositions and part of the $Ttn_2$ compositions documented in titanite from the Sesia marbles (Castelli 1991, and Fig. 3a). In contrast, it is lower than that occurring in HP marble from the Tauern Window and UHP carbonate-bearing eclogite from Dabieshan (Fig. 3a), or in LP high-temperature calc-silicates from the East Antarctic Craton (Markl and Piazolo (1999). The wider scatter in the F vs (Al + $Fe^{3+}$) correlation (Fig. 3b) partly reflects the large error attached to fluorine EDS analysis, but has been also documented in Al-rich titanite from various sources (e.g. Franz and Spear 1985; Enami et al. 1993; Carswell et al. 1996; Markl and Piazolo 1999).

Chemical data on single titanite crystal (Fig. 4), BSE images and X-ray elemental maps (Fig. 2) show that substitution (1) cannot be simply related to regular zoning from the core to rim. In both samples, euhedral to subhedral titanites that are isolated in the calcite matrix (Fig. 2a; crystals SL1821-6, SL1821-8 and SL1823/PA-8 in Fig. 4) may have different Al contents, but substitution (1) occurs in a narrow range, with gradational boundaries between different compositional domains. In contrast, subhedral to anhedral, often deformed and/or fractured crystals in contact with (or rimmed by) omphacite ± phengite and quartz are patchy zoned, with sharper boundaries between different compositional domains, which are characterized by larger amounts of substitution (1). In particular, lower Al contents occur either at the contact between titanite and HP minerals (e.g. Fig. 2c, d) or along lobate boundaries of partly resorbed titanite (Fig. 2b). In sample SL1821 (Fig. 4), the larger substitution range has been observed in crystal #1821-1 ($0.148 < X_{Al} < 0.248$); whereas, in sample SL1823/PA, it occurs in crystal #PA-5 ($0.188 < X_{Al} < 0.332$). As mentioned above, F chiefly correlates with Al within single crystals (Fig. 3b, see also F values in Fig. 2) and, in many X-ray maps, the distribution pattern of F closely match that of Al. However, calculated $X_F = F/(F + OH)$ values are in the range 0.28–0.98 (av. = 0.60 and 0.58 in samples SL1821 and SL1823/PA, respectively), showing that Al substitution

**Table 2** Representative spot analyses of titanite. Analysis are listed in order of increasing $Al_2O_3$ content. The site label refers to location of SHRIMP analysis. *n.m.* Not measured. Cations calculated according to Oberti et al. (1991); total corrected for F, if measured; all Fe as $Fe^{3+}$

| Sample | SL1821 | | | | | SL1823/PA | | | | | Uncertainties (3 $\sigma$) |
|---|---|---|---|---|---|---|---|---|---|---|---|
| site: no. analysis | 1821-1.2 61123 | 1821-1.1 1821-1-E | 1821-6.2 61120 | 1821-8.1 61126 | 1821-6.1 61119 | PA-8.1 61117 | PA-5.3 61116 | PA-9.1 61118 | PA-1.5 61105 | PA-5.2 61114 | |
| $SiO_2$ | 30.93 | 30.68 | 31.35 | 31.62 | 31.41 | 31.48 | 30.75 | 31.10 | 31.54 | 31.52 | $\pm$ 0.26 |
| $TiO_2$ | 34.17 | 31.56 | 29.04 | 28.68 | 28.10 | 31.81 | 32.12 | 31.40 | 29.28 | 28.18 | $\pm$ 0.40 |
| $Al_2O_3$ | 4.31 | 6.36 | 8.16 | 8.24 | 9.02 | 5.72 | 6.26 | 6.71 | 7.59 | 9.08 | $\pm$ 0.31 |
| $Fe_2O_3$ | 0.01 | 0.42 | 0.16 | 0.26 | 0.15 | 0.43 | 0.00 | 0.51 | 0.59 | 0.44 | $\pm$ 0.10 |
| MnO | 0.14 | 0.09 | 0.00 | 0.00 | 0.01 | 0.01 | 0.00 | 0.07 | 0.25 | 0.13 | n.c. |
| MgO | 0.11 | 0.10 | 0.09 | 0.11 | 0.00 | 0.01 | 0.02 | 0.05 | 0.18 | 0.00 | n.c. |
| CaO | 28.43 | 29.22 | 28.61 | 28.98 | 29.12 | 28.38 | 28.77 | 28.47 | 28.35 | 29.22 | $\pm$ 0.28 |
| $Na_2O$ | 0.03 | 0.02 | 0.10 | 0.04 | 0.09 | 0.16 | 0.07 | 0.00 | 0.20 | 0.00 | n.c. |
| $K_2O$ | 0.09 | 0.07 | 0.00 | 0.06 | 0.09 | 0.00 | 0.00 | 0.02 | 0.03 | 0.01 | n.c. |
| F | 0.99 | n.m. | 1.86 | 1.60 | 2.23 | 0.93 | 0.99 | 1.80 | 1.10 | 2.53 | $\pm$ 0.51 |
| Total | 98.79 | 98.52 | 98.59 | 98.92 | 99.28 | 98.54 | 98.56 | 99.37 | 98.65 | 100.05 | |
| Si | 1.000 | 0.980 | 1.000 | 1.000 | 1.000 | 1.000 | 0.998 | 1.000 | 1.000 | 1.000 | |
| Ti | 0.831 | 0.758 | 0.697 | 0.682 | 0.673 | 0.760 | 0.784 | 0.759 | 0.698 | 0.672 | |
| Al | 0.164 | 0.239 | 0.307 | 0.307 | 0.338 | 0.214 | 0.239 | 0.254 | 0.284 | 0.340 | |
| $Fe^{3+}$ | 0.000 | 0.010 | 0.004 | 0.006 | 0.004 | 0.010 | 0.000 | 0.012 | 0.014 | 0.010 | |
| Ca | 0.985 | 1.000 | 0.978 | 0.982 | 0.993 | 0.966 | 1.000 | 0.981 | 0.963 | 0.993 | |
| $\Sigma$ cations | 2.980 | 2.987 | 2.986 | 2.977 | 3.008 | 2.950 | 3.021 | 3.006 | 2.959 | 3.015 | |
| O | 4.787 | 4.701 | 4.674 | 4.633 | 4.704 | 4.646 | 4.844 | 4.799 | 4.612 | 4.727 | |
| F | 0.104 | | 0.196 | 0.168 | 0.235 | 0.098 | 0.104 | 0.189 | 0.116 | 0.266 | |
| OH | 0.109 | | 0.130 | 0.198 | 0.061 | 0.256 | 0.051 | 0.011 | 0.272 | 0.007 | |
| $\Sigma Ti + Al + Fe^{3+}$ | 0.995 | 1.007 | 1.008 | 0.996 | 1.015 | 0.984 | 1.023 | 1.025 | 0.996 | 1.022 | |
| $X_{Ti}$ | 0.835 | 0.753 | 0.691 | 0.685 | 0.663 | 0.772 | 0.766 | 0.740 | 0.701 | 0.658 | |
| $X_{Al}$ | 0.165 | 0.238 | 0.305 | 0.309 | 0.333 | 0.218 | 0.234 | 0.248 | 0.285 | 0.332 | |
| $X_F$ | 0.488 | | 0.601 | 0.459 | 0.794 | 0.277 | 0.671 | 0.945 | 0.299 | 0.973 | |

in these titanites is also coupled to extensive substitution of $O^{2-}$ by $OH^-$.

Sensitive high-resolution ion microprobe U–Pb analyses of titanite from samples SL1821 and SL1832/PA scatter over a wide range (Table 3 and Fig. 5). The uncorrected data do not lie on a single regression line toward common Pb in the measured $^{207}Pb/^{206}Pb$ vs $^{238}U/^{206}Pb$ plot (Fig. 5a), which prevents the calculation of the common Pb composition. Therefore, the correction for common Pb has been done on the basis of a model composition (Stacey and Kramers 1975; see analytical techniques for further details on common Pb correction). The $^{206}Pb/^{238}U$ ratios (corrected for common Pb) range from 0.0240 to 0.0449 and correspond to apparent ages between 259 and 203 Ma for sample SL1832/PA and between 283 and 153 Ma for sample SL1821. Despite the large percentage of common Pb within some of the analyses, there is no direct correlation between the amount of common Pb and age (Fig. 5b), which indicates that the spread of ages is not an artefact of the common Pb correction applied. These ages cover the same spectrum found by Schärer et al. (1999) with a isotope dilution technique of titanite multigrain fractions. In both samples, the age interval is larger than the spread expected considering the analytical uncertainties alone, and most of the ages are analytically discordant
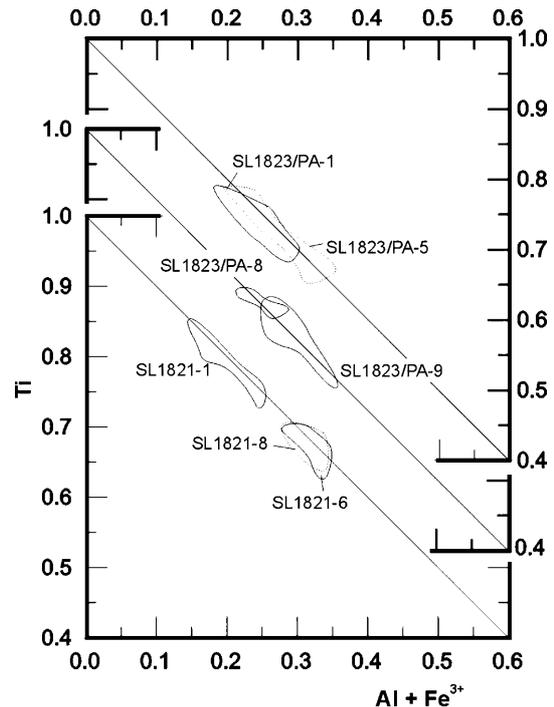


**Fig. 4** Detail of correlation between (Al + $Fe^{3+}$) and Ti (per formula unit) in analysed titanite domains of Table 1. Each *field* contours the chemical variation within a single titanite crystal. *Straight lines* as in Fig. 3. See text for discussion

**Table 3** SHRIMP U–Th–Pb analyses of titanite (uncertainties at $1\sigma$ level) and $X_{Al}$ values at SHRIMP pits

| Label | Th/U | %Pb$^{comm}$ | Measured ratios | | | Radiogenic ratios | | | Apparent ages (Ma) | | | $X_{Al}$ (range) | $X_{Al}$ (av.) |
|---|---|---|---|---|---|---|---|---|---|---|---|---|---|
| | | | $^{204}Pb/^{206}Pb$ | $^{207}Pb/^{206}Pb$ | $^{208}Pb/^{206}Pb$ | $^{207}Pb/^{206}Pb$ | $^{207}Pb/^{235}U$ | $^{206}Pb/^{238}U$ | Age $^{207}Pb/^{206}Pb$ | Age $^{207}Pb/^{235}U$ | Age $^{206}Pb/^{238}U$ | | |
| SL1823/PA-1.2 | 0.005 | 14.00 | 0.0077±0.0009 | 0.149±0.009 | 0.233±0.023 | 0.0343±0.0193 | 0.158±0.089 | 0.0335±0.0013 | – | 149±84 | 213±8 | 0.240–0.252 | 0.246 |
| SL1823/PA-1.3 | 0.355 | 8.92 | 0.0049±0.0004 | 0.151±0.016 | 0.323±0.038 | 0.0825±0.0188 | 0.414±0.095 | 0.0364±0.0012 | 1,258±446 | 352±81 | 230±7 | 0.237–0.249 | 0.243 |
| SL1823/PA-1.4 | 0.001 | 11.01 | 0.0060±0.0012 | 0.135±0.010 | 0.214±0.022 | 0.0461±0.0229 | 0.231±0.115 | 0.0363±0.0015 | 4±1198 | 211±105 | 230±9 | 0.238–0.250 | 0.243 |
| SL1823/PA-1.5 | 0.316 | 9.30 | 0.0051±0.0005 | 0.123±0.008 | 0.246±0.018 | 0.0479±0.0122 | 0.226±0.058 | 0.0342±0.0011 | 94±603 | 207±53 | 217±7 | 0.271–0.285 | 0.279 |
| SL1823/PA-5.1 | 0.635 | 1.22 | 0.0007±0.0001 | 0.062±0.001 | 0.172±0.003 | 0.0526±0.0016 | 0.290±0.013 | 0.0401±0.0012 | 310±71 | 259±11 | 253±8 | 0.302–0.314 | 0.310 |
| SL1823/PA-5.2 | 0.630 | 1.65 | 0.0009±0.0001 | 0.064±0.001 | 0.177±0.002 | 0.0509±0.0018 | 0.288±0.013 | 0.0410±0.0012 | 235±84 | 257±12 | 259±7 | 0.298–0.332 | 0.316 |
| SL1823/PA-5.3 | 0.476 | 2.24 | 0.0012±0.0001 | 0.065±0.001 | 0.150±0.002 | 0.0470±0.0027 | 0.212±0.014 | 0.0327±0.0010 | 49±135 | 195±12 | 207±6 | 0.219–0.246 | 0.233 |
| SL1823/PA-14.1 | 0.124 | 5.32 | 0.0029±0.0004 | 0.089±0.002 | 0.124±0.004 | 0.0455±0.0068 | 0.227±0.035 | 0.0362±0.0013 | – | 208±32 | 229±7 | Not measured | – |
| SL1823/PA-8.1 | 0.062 | 25.88 | 0.0142±0.0010 | 0.236±0.013 | 0.479±0.028 | 0.0000±0.0000 | 0.000±0.000 | 0.0320±0.0013 | – | – | 203±8 | 0.216–0.218 | 0.217 |
| SL1823/PA-9.1 | 0.043 | 5.58 | 0.0031±0.0006 | 0.095±0.004 | 0.118±0.005 | 0.0500±0.0103 | 0.232±0.049 | 0.0337±0.0011 | 193±480 | 212±44 | 214±7 | 0.248–0.256 | 0.252 |
| SL1821-1.1 | 0.271 | 18.64 | 0.0102±0.0013 | 0.198±0.011 | 0.429±0.033 | 0.0477±0.0268 | 0.212±0.120 | 0.0322±0.0013 | 86±1333 | 195±110 | 205±8 | 0.238–0.248 | 0.243 |
| SL1821-1.2 | 0.176 | 36.57 | 0.0200±0.0021 | 0.273±0.009 | 0.576±0.017 | 0.0729±0.0118 | 0.241±0.040 | 0.0240±0.0008 | 1,010±329 | 220±36 | 153±8 | 0.148–0.168 | 0.159 |
| SL1821-6.1 | 0.366 | 0.97 | 0.0005±0.0001 | 0.060±0.001 | 0.108±0.002 | 0.0519±0.0016 | 0.322±0.014 | 0.0449±0.0013 | 282±69 | 283±12 | 283±8 | 0.333–0.339 | 0.336 |
| SL1821-6.2 | 0.674 | 3.56 | 0.0019±0.0006 | 0.084±0.010 | 0.241±0.025 | 0.0551±0.0134 | 0.335±0.082 | 0.0441±0.0014 | 418±544 | 294±72 | 278±8 | 0.305–0.319 | 0.312 |
| SL1821-8.1 | 0.373 | 2.23 | 0.0012±0.0002 | 0.066±0.001 | 0.128±0.003 | 0.0479±0.0029 | 0.262±0.018 | 0.0397±0.0012 | 92±144 | 236±16 | 251±7 | 0.309–0.322 | 0.315 |
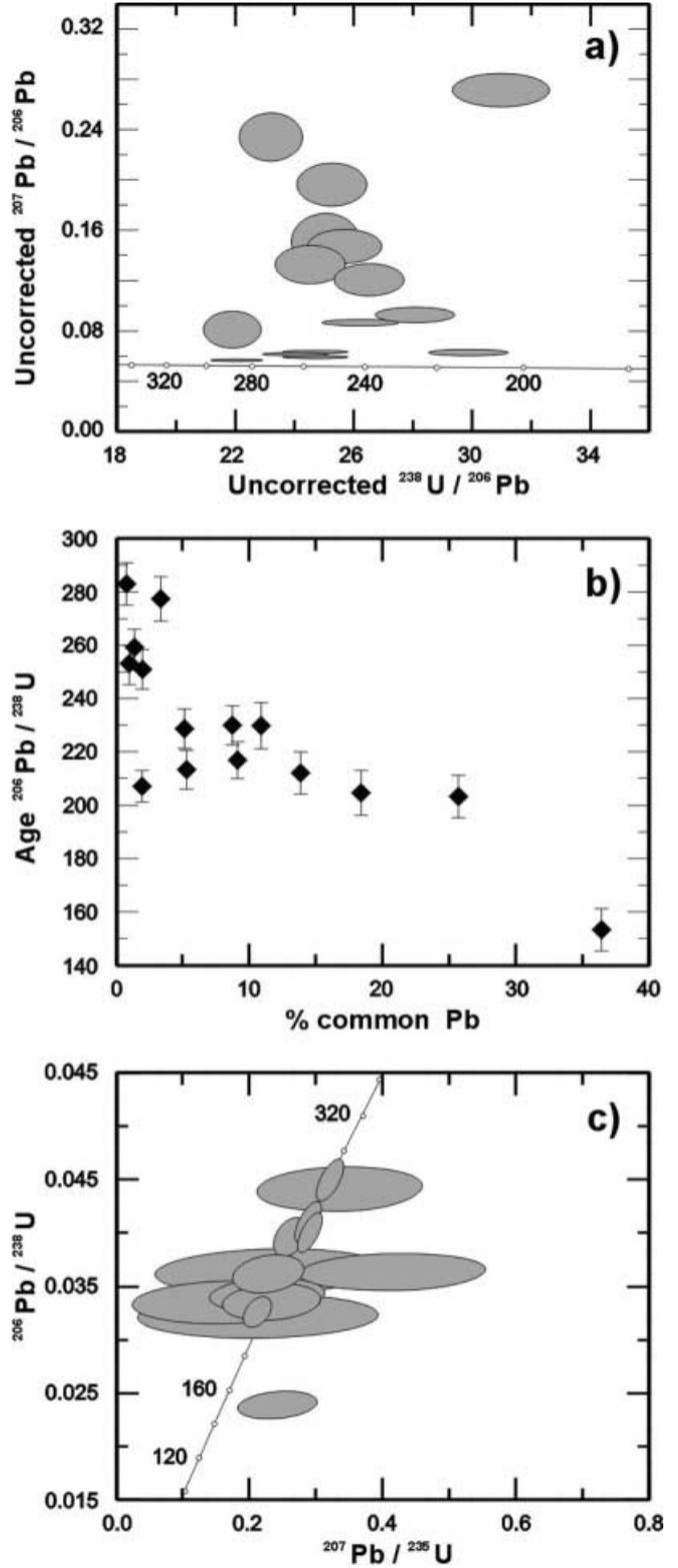


(Table 3) and spread along the concordia (Fig. 5a, c). Therefore, the data cannot be considered a homogeneous population hence preventing the calculation of a geologically meaningful age for this titanite formation. However, the combination of chemical and isotopic

◄

**Fig. 5** SHRIMP U–Pb analyses of titanites from samples SL 1821 and SL 1823/PA. **a** Inverted concordia diagram for uncorrected data. The analyses scatter and do not plot on a single regression line from common Pb. **b** Apparent $^{206}Pb/^{238}U$ age versus percent of common Pb showing that no simple correlation exists between age and common Pb in each analysis. **c** Conventional concordia diagram showing a dispersion of the data along concordia. The data have a large uncertainty on the $^{207}Pb/^{235}U$ ratio because of the low amount of radiogenic $^{207}Pb$ in such young and low U titanites. Because of this large uncertainty and the reduced curvature of the concordia in this interval, most analyses appear concordant even though are geologically meaningless

data from the domains dated deserves some important comments.

There is a positive correlation between the $^{206}Pb/^{238}U$ ratio and the Al content in titanite (Fig. 6), but the $X_{Al}$ data (Table 3) indicate that some of the areas analysed by SHRIMP are heterogeneous at a very fine scale. Thus, it is likely that the 25-μm SHRIMP spot was not small enough to sample the end members in terms of Al composition. However, the data clearly indicate that the oldest titanite domains are Al-rich, with progressively younger titanite at lower Al contents. This observation is true for different grains of the same sample, as well as for chemical variations within a single titanite grain. In fact, titanite SL1821-1 (Fig. 2d) has a domain that is particularly poor in Al (0.159 p.f.u.) and yields the youngest age found in the two samples ($153 \pm 8$ Ma, $1\sigma$), and a domain dated at $205 \pm 8$ Ma ($1\sigma$) with a higher Al content (0.243 p.f.u.). In contrast, titanite SL1821-6 (Fig. 2a) is particularly homogeneous in composition: it has the highest Al content (0.282–0.337 p.f.u.), and two SHRIMP analyses on this grain yielded an age of ∼280 Ma (average $281 \pm 11$ Ma, 95% confidence limit).

## Discussion

### Interpretation of U–Pb data

The scatter in titanite ages beyond analytical uncertainties can be explained in two ways. (1) The titanite U–Pb system was affected by Pb loss because of diffusion after the formation of the titanites at ≥281 Ma, as constrained by the oldest measured age. (2) The measured ages results from the mixing of more than one Pb component: one that was ≥281 Ma old and one younger than ∼153 Ma. The strong chemical zoning of the dated titanites suggests that the titanite crystals underwent a complex re-equilibration history at variable P–T conditions. The age pattern within single crystals is not likely to have been produced by simple outward diffusion of Pb, which would have produced younger rims and older cores. Experimental (Cherniak 1993), theoretical (Dahl 1997) and geochronological studies (e.g. Schärer et al. 1994; Pidgeon et al. 1996; Verts et al. 1996; Essex and Gromet 2000; Rubatto and Hermann 2001) have demonstrated that titanite is able to retain its U–Pb composition at temperatures as high as 750 °C. Therefore, it is to be expected that, if titanite formed in the Sesia marble before Alpine metamorphism, its U–Pb system was not reset or affected by this last thermal event, which occurred at temperatures ≤ 600 °C. Therefore, it seems unlikely that the age scatter was caused by Pb loss from an original ≥281-Ma-old titanite and, thus, the hypothesis of different Pb components within single titanite grains is preferred. The complex chemical and isotopic zoning argues against a new growth of titanite at different stages, which would generate concentric overgrowths. A simple recrystallization process is also unlikely because it would rather have produced a core-

**Fig. 6** $X_{Al}$ vs $^{206}Pb/^{238}U$ (corrected for common Pb) diagrams of titanite. In both diagrams, each *symbol* refers to a single titanite crystal, and different domains where SHRIMP analyses are provided within the same crystal are labelled as in Tables 1 and 3, and Fig. 4. Changes in $X_{Al}$ within each domain are shown by SEM-EDS spot analyses; *vertical bars* are relative error ($1\sigma$) from Table 3. Total $R = 0.9388$ ($n = 41$)
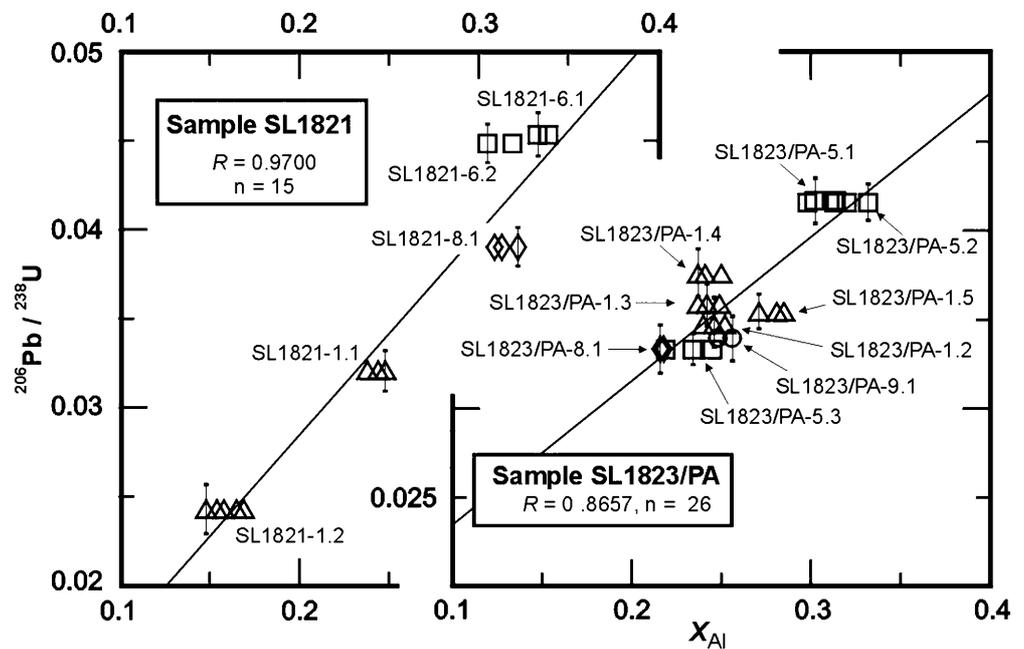
rim structure as observed in zircon from the Sesia Zone (Rubatto et al. 1999) and in titanite from the Dora Maira, an Alpine unit that underwent a similar polymetamorphic evolution at higher temperature (Rubatto and Hermann 2001). Therefore, it is suggested that the studied titanites were formed during pre-Alpine times and that, later, they underwent a partial re-equilibration process that affected both major elements and the U–Pb system.

Inger et al. (1996) previously suggested the presence of different generations of Alpine and Variscan titanite in the Sesia rocks in order to justify the ages of 141 and 107 Ma obtained by U–Pb multigrain analyses. The extensive use of microanalytical techniques does allow a better insight into the chemical processes that lead to these mixing ages. Our data suggest that the chemical zoning is at a finer scale than the 25-μm of the SHRIMP analysis pit and, as a consequence, the true ages of formation and re-equilibration were not necessarily measured. However, the oldest age measured ($281 \pm 11$ Ma; grain #1821-6, Fig. 2c) represents a minimum age for the formation of Al- and F-rich titanite in the Sesia marble. Thus, from the geology and petrology of the sample it is likely that titanite formed during HT Variscan metamorphism, whose age is around 300 Ma (Reddy et al. 1996; Rubatto 1998; see also the section Geological setting). Chemical and isotopic re-equilibration must have occurred during one or more post-Variscan events, the youngest of which must be $\leq 153$ Ma. Because no tectono-metamorphic or magmatic event is recorded in the Sesia Zone between the Variscan and the Alpine metamorphism, it is likely that titanite re-equilibration occurred during this last event, whose HP stage was previously dated at ~65 Ma (Inger et al. 1996; Duchêne et al. 1997; Rubatto et al. 1999, see the section Geological setting).

Petrologic modelling

Based on micro-textural relationships, Castelli (1991) ascribed the Al- and F-rich titanites in the Sesia marbles to the HP Alpine metamorphic stage (in agreement with then available data on both experimental and natural HP titanites: Smith 1977, 1980, 1981; Smith and Lappin 1982; Franz and Spear 1985; Oberti et al. 1985, 1991). However, the above chemical and isotopic data suggest that the Al- and F-rich titanite in the polymetamorphic Sesia marble formed during the HT–LP Variscan metamorphism, most probably favoured by appropriate fluid and bulk rock compositions. During the Alpine subduction and metamorphic climax, the physicochemical conditions of the HP stage were likely to keep the titanite as a refractory system, apart for local re-equilibration. This interpretation is supported by recent data (e.g. Enami et al. 1993; Carswell et al. 1996; Markl and Piazolo 1999) showing that the Al content of titanite is dependent not only on P and T, but also on the activity

of F. Gibert et al. (1990, their Fig. 4) and Markl and Piazolo (1999, their Fig. 8) have also demonstrated the dependence of titanite composition on both $TiO_2$ and $Al_2O_3$ activity, in addition to F activity. Local, Alpine chemical re-equilibration of titanite could have been partially driven by textural relationships with other silicates growing at the HP stage. Within the same crystal, titanite domains in contact with omphacite and/or phengite are often Al-poor (e.g. Fig. 2b, d), whereas isolated titanite in the calcite matrix is more homogeneous (Fig. 2a). The Al- and F-titanite was possibly an additional source for Al in HP clinopyroxene: omphacite in both SL1821 and SL1823/PA samples only occurs close to titanite (see Table 1, and Fig. 2b–d), whereas HP clinopyroxene in equilibrium with garnet at the rim of pre-Alpine salite is lower in the jadeite component.

The lack of pre-Alpine, titanite-bearing equilibrium assemblages hampers precise modelling of bulk composition and coexisting fluid. However, some reasonable assumptions help to constrain the P–T–$X_{fluid}$ conditions for the formation and stability of Al, F titanite by using phase equilibria calculation and inferred P–T conditions of both pre-Alpine and Alpine metamorphic events in the internal Sesia Zone (Fig. 7). In particular, (1) compositions of the relevant minerals may be essentially modelled in the CaO–$TiO_2$–$SiO_2$ system; (2) the fluid phase that probably coexisted with the above minerals at lithostatic pressure may be modelled as a binary $H_2O$–$CO_2$ fluid (Castelli 1991); (3) aragonite occurred instead of calcite during the HP Alpine event; (4) both rutile and wollastonite have never been observed at any metamorphic stage; and (5) the scanty occurrence of graphite in the marbles cannot be directly related to any titanite-forming stage.

Selected phase equilibria have, therefore, been calculated in the CaO–$TiO_2$–$SiO_2$–$H_2O$–$CO_2$ model system, using the approach of Connolly (1990) with the thermodynamic mineral data and the CORK equation of state for the $H_2O$–$CO_2$ fluids of Holland and Powell (1998). Aragonite, calcite, quartz, rutile and wollastonite were treated as pure phases. Titanite was considered both at ideal and true composition. The occurrence of ideal titanite may be modelled after the equilibrium:

$$Rt + Cal/Arg + Qtz = Ttn + CO_2 \qquad (2)$$
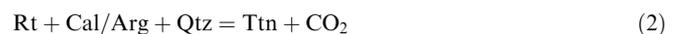
Calculations show that $H_2O$-rich fluid enlarges the titanite stability field (Fig. 7a). The solution model of Ghent and Stout (1994) has been also used to calculate the shift of equilibrium (2) as a result of coupled substitution (1) in titanite. At $a^{Ttn}_{CaTiSiO_5} = 0.65$, and constant temperature and fluid composition, the ΔP of reaction (2) is larger at high temperature and $CO_2$-rich conditions (i.e. ΔP = 3,760 bar, at T = 750 °C and $X_{CO_2} = 1$) than at low T and $H_2O$-rich conditions (i.e. ΔP = 2,690 bar, at T = 500 °C and $X_{CO_2} = 0.01$), respectively (Fig. 7a). Our calculations show that, at the inferred P–T conditions of the pre-Alpine metamorphic event, any titanite composition is more stable than the Rt + Cal + Qtz assemblage, for any $X_{CO_2}$ value of the binary fluid (Fig. 7a, c).
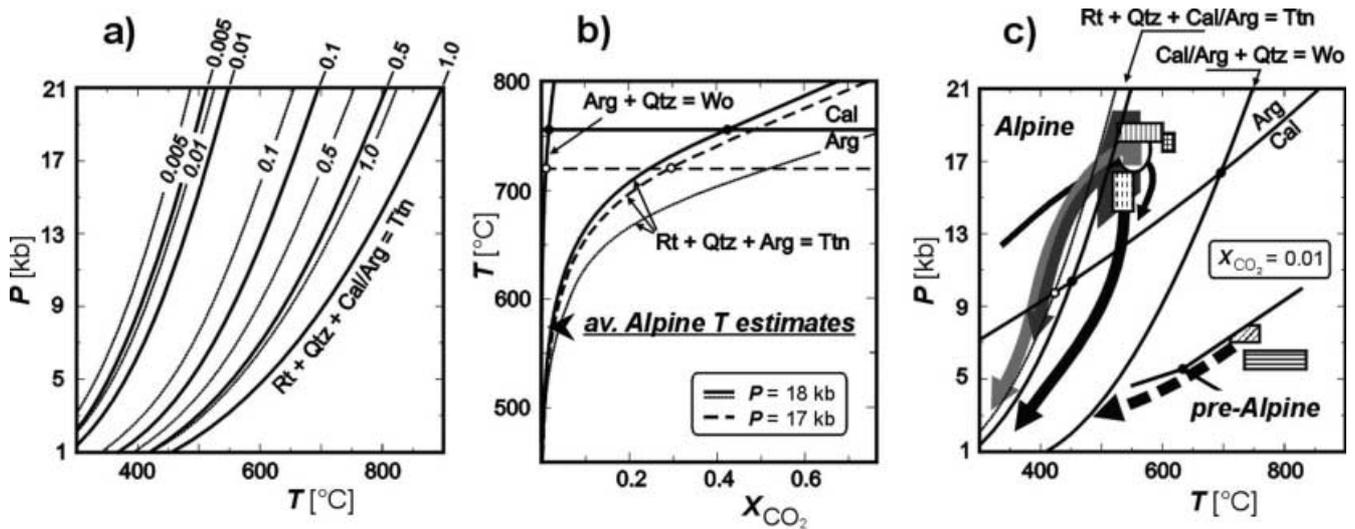
**Fig. 7 a** P–T loci of the univariant equilibrium Rt + Arg/Cal + Qtz = Ttn at different fluid compositions (numbers are $X_{CO_2}$ values) in the model system CaO–TiO$_2$–SiO$_2$–H$_2$O–CO$_2$. *Solid thick curves* refer to calculations where minerals are treated as pure phases. *Dotted thin curves* show shifts of the equilibrium for the same fluid compositions at $a_{CaTiSiO_5}^{Ttn} = 0.65$. **b** Polibaric T–$X_{CO_2}$ diagram for the same system, showing univariant equilibria relevant for the stability of the titanite–aragonite–quartz assemblage at P = 18 kbar (*solid thick curves*) and at P = 17 kbar (*dashed thick curves*). The *dotted thin curve* shows the shift of equilibrium Rt + Arg/Cal + Qtz = Ttn toward higher CO$_2$-rich conditions at P = 18 kbar and $a_{CaTiSiO_5}^{Ttn} = 0.65$. The stability field of aragonite is limited by wollastonite and calcite stability. The *arrow* points to average T estimates of the high-pressure Alpine stage in metacarbonates (Castelli 1991, and this study). Calculations and analysis in **a** and **b** according to Connolly (1990) and Castelli et al. (1997), using the thermodynamic data of Holland and Powell (1998). Reaction equations are written such that the high-T assemblage is on the products side. **c** Selected univariant equilibria from **a** and **b** are plotted with pre-Alpine and Alpine P–T paths and estimates of the internal Sesia Zone. The *dotted thin curve* shows the shift of equilibrium Rt + Arg/Cal + Qtz = Ttn at $a_{CaTiSiO_5}^{Ttn} = 0.65$. The pre-Alpine path (*dashed thick arrow*) is from Lardeaux and Spalla (1991). *Boxes with oblique and horizontal ornaments* show P–T estimates of pre-Alpine metamorphism from Lardeaux and Spalla (1991) and Pognante (1989), respectively (the stability fields of Al$_2$SiO$_5$ polymorphs are shown as reference). Alpine paths according to Lardeaux et al. (1982, *solid thick arrow*), Pognante (1989, *dark grey arrow*), Pognante (1991, *pale grey arrow*) and Rubbo et al. (1999, *solid thin arrow*). P–T estimates of the high-pressure Alpine stage are from Compagnoni (1977, *white field*), Koons (1982, *box with grid*) Lardeaux et al. (1982, *box with dashed vertical ornament*), Pognante (1989, 1991, *dark and pale grey field*, respectively), and this study (*box with vertical ornament*). See text for discussion

This proves that the Al- and F-rich titanite could have formed during the pre-Alpine stage, albeit the fluid composition is only documented in the binary H$_2$O–CO$_2$ system.

During the HP Alpine stage, the occurrence of titanite instead of rutile is better constrained by equilibrium (2), as the stability of titanite requires very aqueous-rich compositions of the coexisting fluid. Particularly, based on inferred P–T conditions of this stage, in both the polymetamorphic marble (T = 573 ± 23 °C at P = 18 kbar) and country rocks (Fig. 7b, c), a coexisting fluid with $X_{CO_2} \leq 0.01$ is modelled, which is in agreement with $X_{CO_2}$ estimates in Sesia marbles by Castelli (1991).

The modelled P–T–$X_{CO_2}$ conditions would allow most of the pre-Alpine Al- and F-rich titanite crystals to be preserved during HP Alpine overprint and, hence, to maintain their pre-Alpine $^{206}$Pb/$^{238}$U signature, as observed in many euhedral to subhedral titanite crystals. The later P–T path followed by the Sesia rocks almost overlaps equilibrium (2), depending on titanite and/or fluids composition (Fig. 7c). As the P–T exhumation paths of Pognante (1989, 1991) are based on the heterogeneous occurrence of retrograde lawsonite in the southern part of the internal Sesia Zone, the alpine P–T path of Lardeaux et al. (1982) is likely to be closer to the actual exhumation path followed by the polymetamorphic marble. This points to P–T–$X_{CO_2}$ conditions during exhumation that are in the stability field of titanite, as documented by the lack of rutile and the widespread occurrence of low-Al neoblastic titanite in marbles from the same area (Castelli 1991).

## Conclusions

BSE investigations, X-ray elemental maps and SEM-EDS analyses show that chemical composition of titanite in the Sesia polymetamorphic marble is highly heterogeneous. The amount of Al$_1$(F, OH)$_1$Ti$_{-1}$O$_{-1}$ substitution is variable, even within single crystals, and mainly occurs at grain boundaries with HP Alpine phases such as omphacite and phengite. In contrast, most of the titanite crystals that are isolated in the carbonate matrix are rather homogeneous in composition and have higher Al and F contents. The Pb/U values from in-situ SHRIMP analysis on the same titanite crystals also scatter over a wide range, which hampers the calculation of a single age for the titanite formation. However, U–Pb data correlate well with the chemical composition of titanite, which suggests that Pb resetting

was accompanied and most likely driven by chemical re-equilibration at T $\leq$ 600 C.

Petrological observations are the key to the interpretation of a complex U–Pb data set. The age of the titanite crystal that has the most pristine composition (highest Al and F contents) and is most homogeneous represents a minimum age for the formation of Al- and F-rich titanite (281 $\pm$ 11 Ma). Therefore, it appears that the Al- and F-rich titanite formed during a Variscan HT (T = 730–830 °C, P = 7–9 kbar: Lardeaux and Spalla 1991) metamorphic event. On the other hand, the younger age of Al- and F-poor titanite is attributed to partial re-equilibration that most probably occurred during the HP (T = 530–590 °C and P$\sim$18 kbar) Alpine stage dated at $\sim$65 Ma (Rubatto et al. 1999). During Alpine metamorphism, the Al- and F-rich composition of titanite was better preserved in domains with slow reaction kinetics. Here, titanite behaved as an almost refractory system.

Extensive $(Al, Fe^{3+})_1(F, OH)_1 Ti_{-1}O_{-1}$ substitution in titanite is, therefore, not exclusive to HP metamorphic conditions. Our petrologic modelling in the $CaO$–$TiO_2$–$SiO_2$–$H_2O$–$CO_2$ system, combined with independent P–T estimates, indicates that this substitution mechanism may also operate at high temperature, if appropriate bulk composition and high fluorine activity occur. Petrologic modelling and isotopic data also suggests that, at HP conditions and within the quartz stability field, both ideal and Al- and F-rich titanite are the stable Ti phases in carbonate systems.

This approach, which combines petrological and isotopic observations (BSE imaging, X-ray elemental mapping, SEM-EDS and U–Pb in-situ analyses), has proven to be a powerful tool for depicting different stages in the evolution of polymetamorphic samples that are hardly recognizable by conventional isotopic techniques.

# References

Borghi A, Cossio R, Olmi F, Vaggelli G (1998) Compositional X-ray maps of metamorphic and magmatic minerals. Mikrochim Acta (Suppl) 15:227–235

Carswell DA, Wilson RN, Zhai M (1996) Ultra-high pressure aluminous titanites in carbonate-bearing eclogites at Shuanghe in Dabieshan, central China. Mineral Mag 60:461–471

Castelli D (1987) Il metamorfismo alpino delle rocce carbonatiche della Zona Sesia-Lanzo. PhD Thesis, University of Torino, Italy

Castelli D (1988) Chlorpotassium ferro-pargasite from Sesia-Lanzo marbles (Western Italians Alps): a record of highly saline fluids. Rend Soc It Mineral Petrol 43:129–138

Castelli D (1991) Eclogitic metamorphism in carbonate rocks: the example of impure marbles from the Sesia-Lanzo Zone (Italian Western Alps). J Metamorph Geol 9:61–77

Castelli D, Connolly JAD, Franceschi G (1997) VERTEXVIEW: an interactive program to analyze and plot petrological phase diagrams. Comput Geosci 23:883–887

Cherniak DJ (1993) Lead diffusion in titanite and preliminary results on the effects of radiation damage on Pb transport. Chem Geol 110:177–194

Compagnoni R (1977) The Sesia-Lanzo Zone: high pressure–low temperature metamorphism in the Austroalpine continental margin. Rend Soc It Mineral Petrol 33:335–375

Compagnoni R, Dal Piaz GV, Hunziker JC, Gosso G, Lombardo B, Williams PF (1977) The Sesia-Lanzo Zone, a slice of continental crust with alpine high pressure–low temperature assemblages in the western Italian Alps. Rend Soc It Mineral Petrol 33:281–334

Compston W, Williams IS, Kirschvink JL, Zhang Z, Ma G (1992) Zircon U–Pb ages for the Early Cambrian time-scale. J Geol Soc Lond 149:171–184

Connolly JAD (1990) Multivariable phase diagrams: an algorithm based on generalized thermodynamics. Am J Sci 290:666–718

Dahl PS (1997) A crystal–chemical basis for Pb retention and fission-track annealing systematics in U-bearing minerals, with implications for geochronology. Earth Planet Sci Lett 150:277–290

Droop GTR, Lombardo B, Pognante U (1990) Formation and distribution of eclogite facies rocks in the Alps. In: Carswell DA (ed) Eclogite facies rocks. Blackie, Glasgow, pp 225–259

Duchêne S, Blichert-Toft J, Luais B, Télouk P, Lardeaux J-M, Albarède F (1997) The Lu–Hf dating of garnets and the ages of the Alpine high-pressure metamorphism. Nature 387:586–589

Ellis DJ, Green DH (1979) An experimental study of the effect of Ca upon garnet–clinopyroxene Fe–Mg exchange equilibria. Contrib Mineral Petrol 71:13–22.

Enami M, Suzuki K, Liou JG, Bird DK (1993) Al–$Fe^{3+}$ and F–OH substitutions in titanite and constraints on their P–T dependence. Eur J Mineral 5:219–231

Essex RM, Gromet LP (2000) U–Pb dating of prograde and retrograde titanite growth during the Scandian orogeny. Geology 28:419–422

Franz G, Spear FS (1985) Aluminous titanite (sphene) from the eclogite zone, South-Central Tauern Window, Austria. Chem Geol 50:33–46

Frost BR, Chamberlain KR, Schumacher JC (2000) Sphene (titanite): phase relations and role as a geochronometers. Chem Geol 172:131–148

Ghent E, Stout MZ (1994) Geobarometry of low-temperature eclogites: applications of isothermal pressure-activity calculations. Contrib Mineral Petrol 116:500–507

Gibert F, Moine B, Gibert P (1990) Titanites (sphènes) alumineuses formées à basse/moyenne pression dans les gneiss à silicates calciques de la Montagne Noire. C R Acad Sci Paris, Sér II 311:657–663

Hirajima T, Zhang R, Li J, Cong B (1992) Petrology of the nyböite-bearing eclogite in the Donghai area, Jiangsu province, eastern China. Mineral Mag 56:37–46

Holland TJB, Powell R (1998) An internally consistent thermodynamic data set for phases of petrological interest. J Metamorph Geol 16:309–344

Inger S, Ramsbotham W, Cliff RA, Rex DC (1996) Metamorphic evolution of the Sesia-Lanzo Zone, Western Alps: time constraints from multi-system geochronology. Contrib Mineral Petrol 126:152–168

Kinny PD, McNaughton NJ, Fanning CM, Maas R (1994) 518 Ma sphene (titanite) from the Khan pegmatite, Namibia, southwest Africa: a potential ion-microprobe standard. ICOG 8, Berkeley California USA, US Geological Survey Circular 1107

Koons PO (1982) An investigation of experimental and natural high pressure assemblages from the Sesia zone, western Alps, Italy. PhD Thesis, ETH Zürich

Kretz R (1983) Symbols for rock-forming minerals. Am Mineral 68:277–279

Lardeaux JM, Spalla I (1991) From granulites to eclogites in the Sesia Zone (Italian Western Alps): a record of the opening and closure of the Piedmont ocean. J Metamorph Geol 9:35–59

Lardeaux JM, Gosso G, Kienast JR, Lombardo B (1982) Relations entre le métamorphisme et la déformation dans la zone Sesia-Lanzo (Alpes Italiennes). Bull Soc Geol Fr 24:793–800

López Sánchez-Vizcaíno V, Connolly JAD, Gómez-Pugnaire MT (1997) Metamorphism and phase relations in carbonate rocks from the Nevado–Filábride Complex (Cordilleras Béticas, Spain): application of the Ttn + Rt + Cal + Qtz + Gr buffer. Contrib Mineral Petrol 126:292–302

Markl G, Piazolo S (1999) Stability of high-Al titanite from low-pressure calc-silicates in light of fluid and host-rock composition. Am Mineral 84:37–47

Oberhänsli R, Hunziker JC, Martinotti G, Stern WB (1985) Geochemistry, geochronology and petrology of Monte Mucrone: an example of Eo-Alpine eclogitisation of Permian granitoids in the Sesia-Lanzo Zone, Western Alps, Italy. Chem Geol Isotope Geosci Sect 52:165–184

Oberti R, Rossi G, Smith DC (1985) X-ray crystal structure refinement studies of the TiO $\leftrightarrow$ Al(OH,F) exchange in high-aluminium sphenes. Terra Cognita 5:428

Oberti R, Smith DC, Rossi G, Caucia F (1991) The crystal chemistry of high-aluminium titanites. Eur J Mineral 3:777–792

Papageorgakis J (1961) Marmore und Kalksilikatfelse der Zone Ivrea-Verbano zwischen Ascona und Candoglia. Schweiz Mineral Petrogr Mitt 41:157–254

Passchier CW, Urai JL, Van Loon J, Williams PF (1981) Structural geology of the central Sesia Zone. Geol Mijnbow 60:497–507

Pidgeon RT, Bosh D, Bruguier O (1996) Inherited zircon and titanite U–Pb systems in Archean syenite from southwestern Australia: implications for U–Pb stability of titanite. Earth Planet Sci Lett 141:187–198

Pognante U (1989) Lawsonite, blueschist and eclogite formation in the southern Sesia Zone (western Alps, Italy). Eur J Mineral 1:89–104

Pognante U (1991) Petrological constraints on the eclogite and blueschist-facies metamorphism and P–T–t paths in the Western Alps. J Metamorph Geol 9:5–17

Powell R (1985) Regression diagnostics and robust regression in geothermometer/geobarometer calibration: the garnet–clinopyroxene geothermometer revisited. J Metamorph Geol 3:231–243

Reddy SM, Kelley SP, Wheeler J (1996) A 40Ar/39Ar laser probe study of micas from the Sesia Zone, Italian Alps: implications for metamorphic and deformation histories. J Metamorph Geol 14:493–508

Rubatto D (1998) Dating of pre-Alpine magmatism, Jurassic ophiolites and Alpine subductions in the Western Alps. PhD Thesis, ETH Zürich

Rubatto D, Hermann J (2001) Exhumation as fast as subduction? Geology 29:3–6

Rubatto D, Gebauer D, Compagnoni R (1999) Dating of eclogite-facies zircons: the age of Alpine metamorphism in the Sesia-Lanzo Zone (Western Alps). Earth Planet Sci Lett 167:141–158

Rubbo M, Borghi A, Compagnoni R (1999) Thermodynamic analysis of garnet growth zoning in eclogite-facies granodiorite from M. Mucrone, Sesia Zone, Western Italian Alps. Contrib Mineral Petrol 137:289–303

Schärer U, Zhang L-S, Tapponnier P (1994) Duration of strike-slip movements in large shear zones: the Red River belt, China. Earth Planet Sci Lett 126:379–397

Schärer U, Ballèvre M, Castelli D, Féraud G, Ruffet G (1999) Evidence for a single short-lived phase of deep subduction in the Western Alps: new U–Pb and Rb–Sr data. EUG 10, Abstr Vol Terra Abstr 4(1):64–65

Smith DC (1977) Aluminium bearing sphene in eclogites from Sunnmöre (Norway). Geolognytt 10:32–33

Smith DC (1980) Highly aluminous sphene (titanite) in natural high pressure hydrous-eclogite facies rocks from Norway and Italy, and in experimental runs at high pressure, (abstract). 26th Int Geol Congress, Paris

Smith DC (1981) The pressure and temperature dependence of Al-solubility in sphene in the system Ti–Al–Ca–Si–O–H. Progr Exp Petrol NERC Pub Series D-18:193–197

Smith DC, Lappin MA (1982) Aluminium- and fluorine rich sphene and clino-amphibole in the Liset eclogite pod, Norway. Terra Cognita 2:317

Sobolev NV, Shatsky VS (1990) Diamond inclusions in garnets from metamorphic rocks: a new environment for diamond formation. Nature 343:742–746

Stacey JS, Kramer JD (1975) Approximation of terrestrial lead isotope evolution by a two-stage model. Earth Planet Sci Lett 26:207–221

Troitzsch U, Ellis DJ (1999) The synthesis and crystal structure of CaAlFSiO$_4$, the Al–F analog of titanite. Am Mineral 84:1162–1169

Verts LA, Chamberlain KR, Frost CD (1996) U–Pb sphene dating of metamorphism: the importance of sphene growth in the contact aureole of the Red Mountain pluton, Laramie Mountains, Wyoming. Contrib Mineral Petrol 125:186–199

Williams P F, Compagnoni R (1983) Deformation and metamorphism in the Bard area of the Sesia-Lanzo zone, Western Alps, during subduction and uplift. J Metamorph Geol 1:117–140

Ye K, Ye D (1996) Significance of phosphorous (P)- and magnesium (Mg)-bearing high-Al titanite in high pressure marble from Yangguantum, Rongcheng County, Shandong Province. Chin Sci Bull 41:1194–1197